Non-Gravitational Acceleration in the Trajectory of 1I/2017 U1 ('Oumuamua)

Marco Micheli,[1,2] Davide Farnocchia,[3] Karen J. Meech,[4] Marc W. Buie,[5] Olivier R. Hainaut,[6] Dina Prialnik,[7] Norbert Schörghofer,[8] Harold A. Weaver,[9] Paul W. Chodas,[3] Jan T. Kleyna,[4] Robert Weryk,[4] Richard J. Wainscoat,[4] Harald Ebeling,[4] Jacqueline V. Keane,[4] Kenneth C. Chambers,[4] Detlef Koschny,[1,10,11] and Anastassios E. Petropoulos[3]

1. ESA SSA-NEO Coordination Centre, Largo Galileo Galilei, 1, 00044 Frascati (RM), Italy
2. INAF - Osservatorio Astronomico di Roma, Via Frascati, 33, 00040 Monte Porzio Catone (RM), Italy
3. Jet Propulsion Laboratory, California Institute of Technology, 4800 Oak Grove Drive, Pasadena, CA 91109, USA
4. Institute for Astronomy, University of Hawai'i , 2680 Woodlawn Drive, Honolulu, HI 96822, USA
5. Southwest Research Institute, 1050 Walnut Street, Boulder, CO 80302, USA
6. European Southern Observatory, Karl-Schwarzschild-Straß e 2, 85748 Garching bei München, Germany
7. School of Geosciences, Sackler Faculty of Exact Sciences, Tel Aviv University, Ramat Aviv 69978, Israel
8. Planetary Science Institute, 1700 East Fort Lowell Road, Tucson, AZ 85719, USA
9. The Johns Hopkins University Applied Physics Laboratory, Space Exploration Sector, 11100 Johns Hopkins Road, Laurel, MD 20723, USA
10. ESTEC, European Space Agency, Keplerlaan 1, 2201 AZ, Noordwijk, The Netherlands
11. Chair of Astronautics, Technical University of Munich, Boltzmannstraß e 15, 85748 Garching bei München, Germany

Corresponding author: Marco Micheli   marco.micheli@esa.int

Summary

1I/'Oumuamua is the first known object of interstellar origin to have entered the Solar System on an unbound and clearly hyperbolic trajectory with respect to the Sun[1]. A variety of physical observations collected during its short visit to our system showed that the object has an unusually elongated shape and a tumbling rotation state[1,2,3,4], while its surface physical properties resemble those of cometary nuclei[5,6], even though 'Oumuamua showed no evidence of cometary activity[7,5]. The motion of all celestial bodies is mostly governed by gravity, but comet trajectories can also be affected by non-gravitational forces due to cometary outgassing[8]. Since non-gravitational accelerations are at least three to four orders of magnitude weaker than the gravitational acceleration, the detection of any deviation from a purely gravity-driven trajectory requires high-quality astrometry over a long arc and, as a result, non-gravitational effects have been measured on only a limited subset of the small-body population[9]. Here we report the detection, at 30σ significance, of non-gravitational acceleration in the motion of 'Oumuamua. We performed a careful analysis of imaging data from extensive observations by both ground-based and orbiting facilities. This analysis rules out systematic biases and shows that all astrometric data can be described once a non-gravitational component representing a heliocentric radial acceleration proportional to $\sim r^{-2}$ or $\sim r^{-1}$ is included in the model. Exploring physical causes of the observed non-gravitational acceleration of 'Oumuamua, we rule out solar radiation pressure, drag- or friction-like forces, interaction with solar wind for a highly magnetized object, as well as geometric effects originating from 'Oumuamua potentially being composed of several spatially separated bodies or having a pronounced offset between its photocenter and center of mass. However, we find comet-like outgassing to be a physically viable explanation, provided that 'Oumuamua has thermal properties similar to comets.

The object now known as 1I/'Oumuamua was discovered on 2017 October 19 by the Pan-STARRS1 survey[10,11]. Within a few days, additional observations collected with ESA's Optical Ground Station (OGS) telescope and other observatories , together with pre-discovery data from Pan-STARRS1, allowed the determination of a preliminary orbit that was highly hyperbolic (eccentricity of 1.2), identifying the object as originating from outside the Solar System[1] and approaching from the direction of the constellation Lyra, with an asymptotic inbound velocity of ~ 26 km s^{-1}.

The extreme eccentricity of 'Oumuamua's orbit led the Minor Planet Center to initially classify the object as a comet[12]. However, this classification was later withdrawn when imaging obtained immediately after discovery using the Canada-France-Hawaii Telescope (CFHT) and, in the following days, the ESO Very Large Telescope (VLT) and the Gemini South Telescope, both 8-meter-class facilities, found no sign of coma despite optimal seeing conditions (see Fig. 1 and discussion in Methods). In addition, spectroscopic data obtained[7,5] at around the same time showed no evidence of identifiable gas emission in the visible wavelength region of the spectrum. Although the object has a surface reflectivity similar to comets[1,7,5], all other observational evidence available at the time thus suggested that 'Oumuamua was likely inactive

and of asteroidal nature, despite research predicting that cometary interstellar objects should be the easiest to discover[13,1].
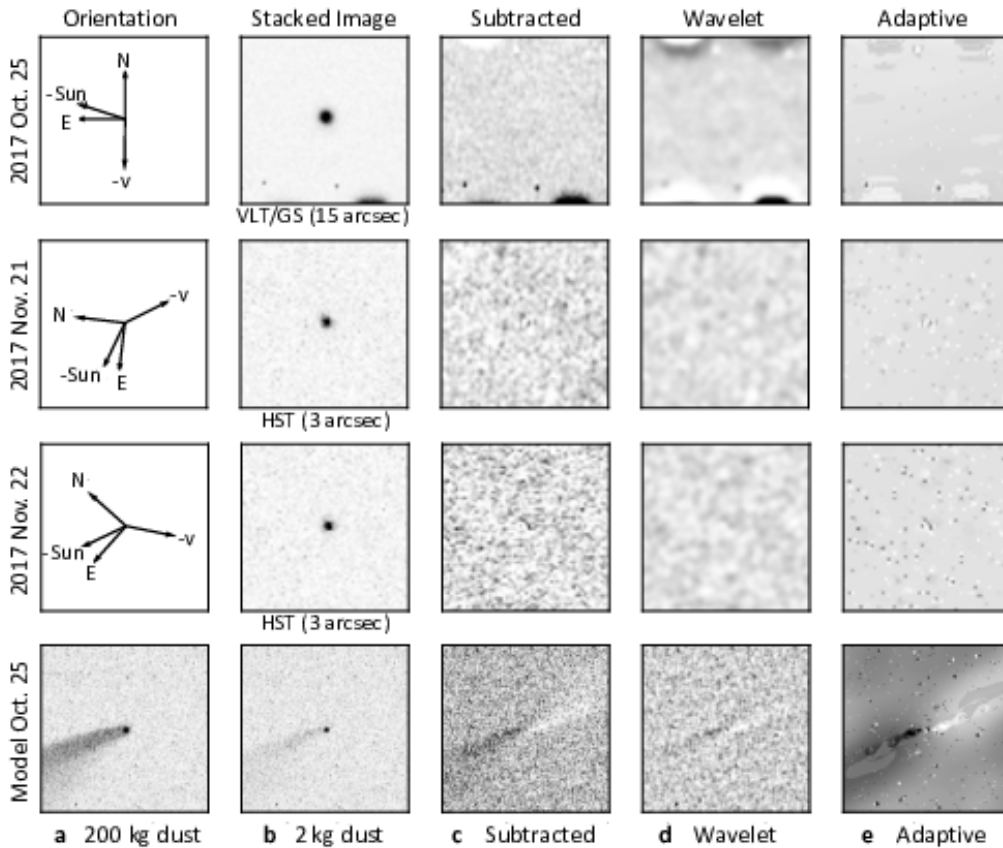

Figure 1. Deep stacked images for dust detection. For each date of observation we show the image orientation (including the anti-solar (-Sun) and anti-motion (-v) directions), the stacked image, a self-subtracted image (see Methods section for details), and the image after application of a wavelet and adaptive filter, respectively, to further enhance low surface brightness features. No dust is visible. To demonstrate the sensitivity of the image enhancement we show a test image, with an artificial cometary feature matching the geometry of the October images. The panels show (a) a very strong feature showing the dust morphology; (b) the same feature scaled to 2 g of dust in the PSF region (i.e. twice the observed 'Oumuamua limit, to ensure its visibility on the figure), (c) (d) (e) processed in the same manner as the real data.

In parallel with physical and compositional studies, our team continued to image 'Oumuamua to further constrain its trajectory through astrometric measurements. As 'Oumuamua faded, we obtained data with CFHT, VLT, and the Hubble Space Telescope (HST; see Methods). A final set of images was obtained with HST in early 2018 for the purpose of extracting high-precision astrometry. The resulting dataset provides dense coverage from discovery to 2018 January 2, when the object became fainter than $V \sim 27$ at a heliocentric distance of 2.9 au.

We carefully analyzed   the full observational dataset, which includes 179 ground-based and 30 HST-based astrometric positions (for a total of 418 scalar measurements) , applying the

procedures and assumptions discussed in the Methods section. Our analysis shows that the observed orbital arc cannot be fit in its entirety by a trajectory governed solely by gravitational forces due to the Sun, the eight planets, the Moon, Pluto, the 16 biggest bodies in the asteroid main belt, and relativistic effects[14]. As shown in the left panel of Fig. 2, the residuals in right ascension and declination of the best-fit gravity-only trajectory are incompatible with the formal uncertainties: ten data points deviate by more than 5σ in at least one coordinate, and 28 are discrepant by more than 3σ. Furthermore, the offsets (as large as $20''$ for the 2017 October 14 Catalina observation) are not distributed randomly but show clear trends along the trajectory.
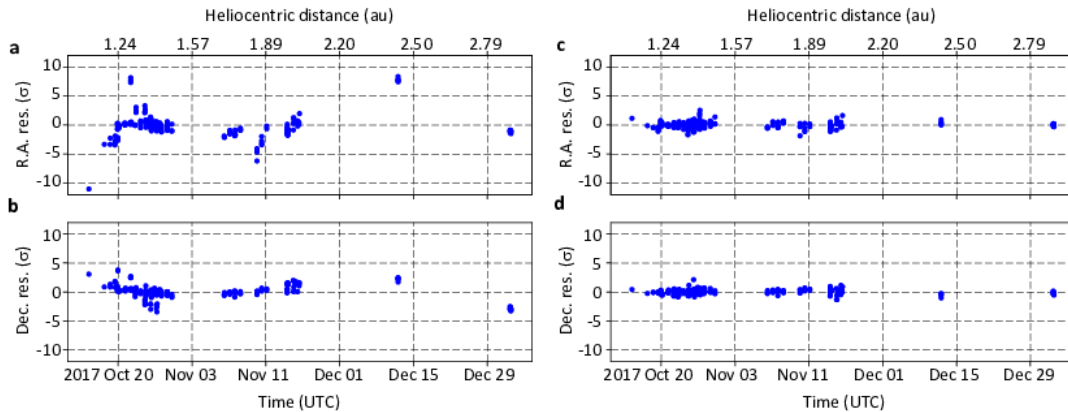

Figure 2. Astrometric residuals of 'Oumuamua observations. a, b: normalized right ascension and declination residuals against a gravity-only solution. c, d: normalized right ascension and declination residuals against a solution that includes a non- gravitational radial acceleration $A_1 r^{-2}$.

To improve the description of 'Oumuamua's trajectory, we included a radial acceleration term $A_1 g(r)$ in the model[8], where A_1 is a free fit parameter, r is the heliocentric distance, and $g(r)$ is set to $\propto r^{-2}$, matching the decrease of solar flux with distance, with $g(1au) = 1$. As shown in the right panel of Fig. 2, the addition of this term allows us to explain the data for a value of A_1 of $(5.01 \pm 0.16) \times 10^{-6}$ m s^{-2}, corresponding to a formal $\sim30\,\sigma$ detection of non-gravitational acceleration. Additional analyses, discussed in greater detail in the Methods section, further support our finding that any non-gravitational acceleration is preferentially directed radially away from the Sun, and allow both the aforementioned r^{-2} dependency and a less steep r^{-1} law. By contrast, constant acceleration independent of distance is strongly disfavored, regardless of direction (either radial, along the instantaneous velocity vector of 'Oumuamua, or inertially fixed). Table 1 reports the χ^2 and χ^2_ν (reduced χ^2) statistics for the astrometric fits of each of the tested models (see the Methods section for details). We used conservative estimates for the measurement uncertainties that serve as data weights in order to mitigate the effect of systematic errors, e.g., due to star catalog biases, field-of-view distortions, clock errors, or the absence of uncertainty information (for astrometry produced by others). As a result, the listed χ^2 and χ^2_ν values are lower than would be expected for purely Gaussian noise, and the correspondingly

larger error bars that we derive more safely capture the actual uncertainties in the estimated parameters.

Table 1. Number of estimated parameters, χ^2 and χ_ν^2 (χ^2 per degree of freedom) for fits of different non-gravitational models to the 'Oumuamuaastrometry. For reference we also list the same values for a gravity-only model of the trajectory. In addition to an impulsive Δv model, we consider continuous non-gravitational accelerations whose dependence on the heliocentric distance r is expressed by the function $g(r)$, which can be a power law or, for H_2O or CO volatiles, based on cometary outgassing models[8,15]. The acceleration vector can be inertially fixed or decomposed in either the Radial, Transverse, Normal (RTN) or the Along-track, Cross-track, Normal (ACN) frame.

Model	# param.	χ^2	χ_ν^2
Gravity-only	6	1082	2.63
1. Impulsive Δv event	10	134	0.33
2. Pure radial acceleration: $A_1 g(r) \propto r^{-k};\ k = 0,1,2,3$	7	100, 86, 91, 113	0.24, 0.21, 0.22, 0.27
3. RTN decomposition: $[A_1, A_2, A_3] g(r) \propto r^{-k};\ k = 0,1,2,3$	9	92, 85, 87, 100	0.23, 0.21, 0.21, 0.25
4. ACN decomposition: $[A_A, A_C, A_N] g(r) \propto r^{-k};\ k = 0,1,2,3$	9	104, 88, 84, 95	0.25, 0.22, 0.21, 0.23
5. Pure along-track acceleration: $A_A g(r) \propto r^{-k};\ k = 0,1,2,3$	7	1082, 1074, 1049, 1007	2.63, 2.61, 2.55, 2.45
6. Constant , inertially fixed, acceleration vector	9	115	0.28
7a. Pure radial acceleration: $A_1 g_{CO}(r)$	7	95	0.23
7b. Pure radial acceleration: $A_1 g_{H_2O}(r)$	7	129	0.32
7c. RTN decomposition: $[A_1, A_2, A_3] g_{CO}(r)$	9	89	0.22
7d. RTN decomposition: $[A_1, A_2, A_3] g_{H_2O}(r)$	9	101	0.25
7e. RTN decomposition: $[A_1, A_2, A_3] g_{H_2O}(r),\ \Delta T$	10	98	0.24

We performed a series of tests, also discussed in greater detail in the Methods section, which confirm that the observed non-gravitational signature is neither an artifact caused by some subset of the observations, nor the result of overall systematic biases unaccounted for in the analysis. Even a substantial inflation of the assumed error bars in the astrometry, applied to reflect possible catalog biases or uncorrected distortions, still results in a significant detection. In addition, the non-gravitational acceleration is clearly detected both in ground-based observations alone and in an HST-only arc complemented with just a few early ground-based high-quality data points.

Exploring a variety of possible explanations for the detected non-gravitational acceleration, we find outgassing to be the most physically plausible explanation, although with several caveats. A thermal outgassing model[16], which treats 'Oumuamua like a common cometary nucleus, creates a non-gravitational force proportional to $\sim r^{-2}$ in the range of distances covered by our observations.

The model predictions for the magnitude and temporal evolution of the non-gravitational acceleration are within a factor of about 2-3 of observations (see Methods)

for a water production rate of $Q_{H_2O} = 4.9 \times 10^{25}$ molecules s^{-1}, or 1.5 kg s^{-1} near 1.4 au and an additional contribution from $Q_{CO} = 4.5 \times 10^{25}$ molecules s^{-1} or 2.1 kg s^{-1}. Outgassing at this level is not in conflict with the absence of spectroscopic limits for outgassing of OH, since the quoted values are well below the spectroscopic limits on production rates[17]. However, the inferred upper limits for water production obtained at 1.4 au based on the non-detection of CN[7] and assumed solar system abundances for Q_{CN}/Q_{OH} [18] show that 'Oumuamua would need to be significantly depleted in CN (by a factor of ~15) relative to water. The model also predicts 0.4 kg s^{-1} of dust production, which should have been detectable in the images. However, if the grains are predominantly larger than a few 100 Âμm to mm they would not have been detected at optical wavelengths (see Methods). In our solar system comet 2P/Encke is noteworthy for its lack of small dust near perihelion[19]. Cometary behavior implies that 'Oumuamua must have some internal strength, at least comparable to Solar System comets[20] since asteroid-like densities are ruled out (see Methods).

Alternative explanations for the observed acceleration proved to be either physically unrealistic or insufficient to explain the observed behavior:

Solar radiation pressure. The simplest physical phenomenon that could cause a radial acceleration following an r^{-2} dependency and directed away from the Sun is pressure from solar radiation, which has indeed been detected for a few small asteroids[21,22,23,24]. However, for 'Oumuamua the magnitude of the observed acceleration implies an unreasonably low bulk density roughly three to four orders of magnitude below the typical density of Solar System asteroids of comparable size. Additional considerations regarding the plausibility of radiation pressure as an explanation for the non-gravitational motion are presented in Methods.

Yarkovsky effect. A rotating body in space experiences a small force due to the anisotropic emission of thermal photons[25]. The resulting perturbation can be excluded as an explanation for the observed acceleration both because of its low intensity (at most comparable to that of solar radiation pressure) and because it mainly affects the motion in the along-track direction, in conflict with our data.

Friction-like effects aligned with the velocity vector. Some dynamical effects, such as friction or drag-like phenomena, tend to be aligned with the direction of motion and not with the heliocentric radial vector. However, decomposition of the non-gravitational acceleration shows that the respective best-fit component along the direction of motion is not only insufficient to explain the observations (see Table 1), but is also positive, while drag-like phenomena would require it to be negative.

Impulsive Δv event. Models of the trajectory that include a single impulsive change in velocity, e.g., due to a collision , provide a poorer fit to the data (Table 1) than purely radial acceleration . More importantly, we see the non-gravitational signal even in disjoint subsets of the observed arc, separated at the time of the possible impulse, which makes continuous acceleration a far more likely explanation.

Binary or fragmented object. In this scenario, the center of mass of the combined system does in fact follow a purely gravitational trajectory, and the detected non-gravitational signature is an artifact, caused by us tracking only the main component of 'Oumuamua. However, no secondary body or fragment is visible in our data down to a few magnitudes fainter than 'Oumuamua, and any object smaller than the corresponding size limit ($\sim$100 times smaller than 'Oumuamua) would be insufficient to explain the observed astrometric offsets.

Photocenter offset. 'Oumuamua may feature surface characteristics that significantly displace the optical photocenter (the point whose position is measured astrometrically) from its center of mass. However, even assuming the longest possible extent of 800 m for a low albedo ($p = 0.04$) object[1] the maximum separation between the two reference points would be approximately $0.005''$ at closest approach, many orders of magnitude less than the observed offset from a gravity-only solution.

Magnetized object. If 'Oumuamua had a strong magnetic field, the interaction with solar wind could affect its motion[26,27]. Assuming a dipole field, a plasma-fluid model, and typical solar wind speed and proton number density[28], we find the resulting acceleration for an object of the nominal size of 'Oumuamua[1] to be only 2×10^{-11} m s^{-2}, i.e., too small by a factor of about 10^5, even if we adopt the high magnetization and density of asteroid (9969) Braille[29].

While this list of possible alternative explanations is not exhaustive, we believe that it covers most physical mechanisms worth exploring based on the data in hand. The models tested in this work attempt only to describe the dynamical behavior of 'Oumuamua within the temporal arc covered by the available observations. The presence of non-gravitational acceleration and the complexity of the physical explanation proposed by us suggest that an extrapolation of 'Oumuamua's past and future trajectory outside the modeled arc may be subject to significant uncertainties.

Outgassing provides the most plausible physical model of the observed non-gravitational acceleration by postulating that 'Oumuamua behaves like a miniature comet. This is consistent with independent results[5,6] showing that the spectra and lack of observed activity are consistent with a cometary body with a thin insulating mantle, and also with the observed non-gravitational accelerations of other Solar System comets (see Fig. 3 in Extended Data). By establishing the object as an icy body (albeit one with possibly unusual chemical composition and dust properties) , this scenario now agrees with the predictions suggesting that only a small fraction of interstellar objects should be asteroidal[30]. The lack of observed dust lifted from the object by the hypothesized cometary activity can be explained by an atypical dust grain size distribution that is devoid of small grains, a low dust-to-ice ratio or surface evolution from its long journey. However, these important aspects of 'Oumuamua's physical nature cannot be resolved conclusively with the existing observations. In-situ observation would be essential to reveal unambiguously the nature, origin, and physical properties of 'Oumuamua and other interstellar objects that may be discovered in the future. This work

shows that while 'Oumuamua looks familiar, there are differences that relate to its birth in a solar system far from our own.

References

[1] Meech, K. J., Weryk, R., Micheli, M., et al.   A brief visit from a red and extremely elongated interstellar asteroid.   *Nature* **552**, 378 (2017).

[2] Fraser, W.C., Pravec, P., Fitzsimmons, A., et al.   The tumbling rotational state of   1I/ 'Oumuamua,   *Nature Astron.* **2**, 383-386 (2018).

[3] Drahus, M., Guzik, P., Waniak, W., et al.   Tumbling motion of of 1I/'Oumuamua reveals body's violent past. *Nature Astron.* **2**, 407-412 (2018).

[4] Belton, M.J.S., Hainaut, O.R., Meech, K.J et al.   The excited spin state of 1I/2017 U1 'Oumuamua,   *ApJL* **856**, L21, (2018).

[5] Fitzsimmons, A., Snodgrass, C., Rozitis, B., et al.   Spectroscopy and thermal modeling of the first interstellar object 1I/2017 U1 'Oumuamua,   *Nature Astron.* **2**, 133-137 (2018)., 133-137 (2018).

[6] Jewitt, D., Luu, J., Rajagopal, J., et al.   Interstellar Interloper 1I/2017 U1: Observations from the NOT and WIYN Telescopes.   *ApJ* **850**, L36 (2017)

[7] Ye, Q.-Z., Zhang, Q., Kelley, M.S.P., Brown, P.G.   1I/2017 U1 ('Oumuamua) is Hot: Imaging, Spectroscopy, and Search of Meteor Activity.   *ApJL* **851**, L5 (2017).

[8] Marsden, B. G., Sekanina, Z., & Yeomans, D. K.   Comets and nongravitational forces. V.   *AJ* **78** 211-225 (1973).

[9] Królikowska, M.   Long-period comets with non-gravitational effects.   *Astronomy and Astrophysics* **427**, 1117-1126 (2004).

[10] Wainscoat, R., et al.   The Pan-STARRS search for Near Earth Objects, in "Asteroids: New Observations, New Models",   *Proceedings IAU Symposium No. 318*, S.R. Chesley, A. Morbidelli, R. Jedicke, and D. Farnocchia eds., 293 (2015)

[11] Denneau, L., et al.   The Pan-STARRS moving object processing system.   *PASP* **125**, 357-395 (2013).

[12] Williams, G.V. MPEC 2017-U181: COMET C/2017 U1 (PANSTARRS). (2017).

[13] Engelhardt, T. et al.   An observational upper limit on the interstellar number density of asteroids and comets. *Astron. J.* **153**, 133 (2017).

[14] Farnocchia, D., Chesley, S. R., Milani, A., Gronchi, G. F., Chodas, P. W.   Orbits, Long-Term Predictions, Impact Monitoring.   *Asteroids IV*, 815-834 (2015).

[15] Yabushita, S.   On the effect of non-gravitational processes on the dynamics of nearly parabolic comets. *MNRAS* **283**, 347-352 (1996).

[16] Prialnik, D. Modeling the Comet Nucleus Interior.   *Earth Moon and Planets*   **89**, 27-52 (2002).

[17] Park, R.S., Pisano, D.J., Lazio, T.J.W., Chodas, P.W., Naidu, S.P. Search for OH 18-cm radio emission from 1I/2017 U1 with the Green Bank telescope.   *AJ* **155**, 85 (2018).

[18] Cochran, A.L., Barker, E.S., Gray, C.L. Thirty years of cometary spectroscopy from McDonald Observatory. *Icarus* **218**, 144-168 (2012).

[19] Fink, U.   A taxonomic survey of comet composition 1985-2004 using CCD spectroscopy.   *Icarus* **201**, 311-334 (2009).

[20] McNeill, A., Trilling, D.E., Mommert, M.   Constraints on the Density and Internal Strength of 1I/'Oumuamua. *ApJ* **857**, L1 (2018)., L1 (2018).

[21] Williams, G.V. MPEC 2008-D12: 2006 RH120. (2008).

[22] Micheli, M., Tholen, D. J., Elliott, G. T.   Detection of radiation pressure acting on 2009 BD.   *New Astronomy* **17**, 446-452 (2012).

[23] Micheli, M., Tholen, D. J., Elliott, G. T.   2012 LA, an optimal astrometric target for radiation pressure detection.   *Icarus* **226**, 251-255 (2013).

[24] Micheli, M., Tholen, D. J., Elliott, G. T. Radiation Pressure Detection and Density Estimate for 2011 MD.   *ApJ* **788**, L1 (2014).

[25] Vokrouhlický, D., Bottke, W. F., Chesley, S. R., Scheeres, D. J., Statler, T. S. The Yarkovsky and YORP Effects. *Asteroids IV*, 509-531 (2015).

[26] Nicole Meyer-Vernet,   *Basics of the Solar Wind,* Cambridge University Press (2007).

[27] Zubrin R.M., Andrews, D.G.   Magnetic Sails and Interplanetary Travel,   *J. Spacecraft and Rockets* **28**, 197-203 (1991).

[28] Wang-Sheeley-Arge (WSA)-Enlil Solar Wind Prediction, Space Weather Prediction Center, www.ngdc.noaa.gov/enlil/, accessed on March 2018.

[29] Richter, I., Auster, H.U., Glassmeier, K.H., et al.   Magnetic field measurements during the ROSETTA flyby at asteroid (21) Lutetia,   *Planetary and Space Science* **66**, 155-164 (2012).

[30] Meech, K. J., Yang, B., Kleyna, J., et al.   Inner solar system material discovered in the Oort cloud.   *Science Advances* **2**, e1600038 (2016)

Author contributions M.M. discovered the non-gravitational acceleration and extracted high-precision astrometry from most ground-based observations obtained by the team. D.F. performed the different fits and modeling of the non-gravitational acceleration. K.J.M. secured the HST time and designed the observations program, computed sublimation dust and gas outgassing limits and provided the assessment of outgassing. M.W.B. led the design of the HST observations and contributed precision astrometry from HST images. O.R.H. obtained the deep stack of images, searched them for dust and companion, and estimated production rates. D.P. performed the thermal sublimation modeling. N.S. conducted thermal model calculations. H.A.W. managed the HST observations and the initial reduction of images. P.W.C. provided support in analyzing possible explanations for the observed non-gravitational acceleration. J.T.K. assembled the deep stack of CFHT data to search for dust and outgassing. R.W. identified and searched pre-discovery images of 'Oumuamua in Pan-STARRS1 data. R.J.W. obtained the observations using CFHT and searched for pre-discovery observations of 'Oumuamua. H.E. contributed to the HST proposal and the design of the HST observations. J.V.K. contributed to the HST proposal. K.C.C. contributed to the HST proposal and text. D.K. provided support in analyzing possible explanations for the observed non-gravitational acceleration. A.E.P. investigated the magnetic hypothesis.

Methods

Ground-based observations. We found the first evidence of non-gravitational forces acting on 'Oumuamua in astrometry derived from a set of ground-based optical images obtained by our team with various ground-based telescopes[1]. Our first optical follow-up observations was performed with ESA's 1.0-meter Optical Ground Station (OGS) in Tenerife, Spain, only 13 hours after 'Oumuamua's discovery. Subsequent deeper observations were conducted with the 3.6-meter Canada-France-Hawaii Telescope (CFHT; seven nights), the 8.2-meter ESO Very Large Telescope, UT1 (VLT; two nights), and the 6.5-meter Magellan Baade telescope (two nights). The astrometric positions derived from this ground-based dataset, together with the associated error bars, are already sufficient to detect the non-gravitational acceleration at the $> 4\sigma$ level.

Search for pre-discovery detections. We searched for pre-discovery images of 'Oumuamua at positions computed from a model trajectory that included the observed non-gravitational acceleration. Pan-STARRS1 observed suitable fields through its broad w-band filter on 2017 June 18 and 22, and through its i-band filter on 2017 June 17, almost three months before perihelion. During this time, 'Oumuamua's predicted average brightness (albeit uncertain due to the large amplitude of the object's lightcurve) was around V~26, significantly fainter than the limiting magnitude of Pan-STARRS1. No object was visible in these images at the predicted location.

HST data and astrometry. Images of 'Oumuamua were obtained with HST in two separate awards of Director's Discretionary (DD) time. The first set of observations was designed soon after 'Oumuamua's discovery, with the primary goal of extending the observational arc in order to obtain tighter astrometric constraints on the object's trajectory . Three HST visits were executed on 2017 November 21-22, one visit was executed on 2017 December 12, and a fifth visit was executed on 2018 January 2. To maximize the length of the covered orbital arc, the last observation was set to be performed as late as possible, assuming that we would know the rotational phase sufficiently well to allow us to catch our steadily fading and only barely detectable target at lightcurve maximum. The discovery of non-principal-axis rotation[2,3,4] invalidated our assumption of a predictable lightcurve and motivated a second allocation of four additional HST orbits, added to the final visit, that allowed us to cover 'Oumuamua in a more sophisticated temporal cadence designed to maximize its detectability regardless of lightcurve phase.

Each visit employed the same basic observing pattern of five 370 s exposures of the full field of WFC3/UVIS, an exposure time that is just long enough to accommodate CCD readout and data storage overheads without loss of integration time within the allocated single orbit. All images were taken through the extremely broad F350LP filter, chosen for maximum throughput. This strategy was modeled after very similar observations of (486958) 2014 MU$_{69}$, the New Horizons extended mission target, and resulted in a signal-to-noise ratio (SNR) of approximately 2 to 3 for a solar-color object of magnitude $R = 27.5$.

During all observations, HST tracked 'Oumuamua, and target motions and parallax corrections were applied. As a result, the object appears as a point source in our images, and the background field stars appear as long trails. As the density of background stars was very low for these observations, the exact placement of our target within the instrument's field of view had to be adjusted for some visits to ensure that the number of reference stars (3 to 10) was sufficient for the aimed-at high-precision astrometric solution.

The positions of reference stars were determined from Point Spread Function (PSF) fitting using the Tiny Tim model[31] and applying a smearing function derived from the HST-centric motion of the object during each exposure. Uncertainties of the resulting position and flux measurements were derived using a Markov Chain Monte Carlo sampling algorithm[32]. The Probability Density Functions (PDFs) from this calculation were then used to update the default World Coordinate System (WCS) solution of each image, using the Gaia DR1[33] position of each star as a reference. A PDF was also derived for this final reference WCS.

The position of 'Oumuamua was computed in the same fashion, except that no smearing function was needed. Object position, flux, and a PDF were derived for each frame where possible (a few images were lost to cosmic-ray strikes). In the final visit, our target was detected in only two of the five orbits. Using the aforementioned WCS PDF for reference, we combined these results to obtain the final sky-plane PDF for the object in each image and then converted the PDF to a Gaussian approximation covariance for use in the fitting of 'Oumuamua's trajectory . While the resulting uncertainties are dominated by catalog errors for the earlier visits, the low SNR of the object contributes significantly to the error budget for the final visit. The formal uncertainties from this procedure reach at most $0.01''$ to $0.02''$, while the absence of proper motions in Gaia DR1 contributes an additional systematic uncertainty of $\sim 0.04''$.

Accumulated observational dataset. Our attempts to constrain the trajectory of 'Oumuamua made use of all available astrometric positions. In addition to our own astrometric dataset (see Tables 2 and 3 in the Extended Data section) , we included all relevant data submitted to the Minor Planet Center, for a total of 179 ground-based observations and 30 HST observations. Seven additional ground-based observations deemed unreliable by the respective observers were not considered. Where no uncertainties were provided by the observers, we assumed a $1''$ positional uncertainty , except for a handful of observations that showed poor internal consistency were further deweighted (these error bars are presented in Table 4 of Extended Data) . Moreover, we assumed that the reported observation times are uncertain by 1 s. Finally, positions that did not use the Gaia DR1 catalog[33] as reference were corrected for systematic errors of the respective star catalog[34], resulting in corrections as large as $0.4''$ for the USNO-B1.0 catalog[35].

Potential biases in the detection of non-gravitational motion. To test whether the detected non-gravitational acceleration could be an artifact introduced by a subset of biased astrometric observations, we used the $A_1 g(r)$, $g(r) \propto r^{-2}$ non-gravitational model and

performed a series of analyses on subsets of the full data arc, designed to highlight whether specific groups of observations could be responsible for the signal. A summary of our findings shows:

The signal is not caused by the early, noisier observations. Fitting only data taken after 2017 October 25, or after 2017 November 15, still yields a detection of A_1 at 18σ and 3.5σ confidence, respectively.

Similarly, the signal is not caused only by the late part of the arc. Fitting only data taken prior to 2017 November 15, or up to 2017 December 1, still yields a detection of A_1 at 3.0σ and 7.3σ confidence, respectively.

To rule out biases in data from ground-based observations, e.g., due to color refraction in the atmosphere, we computed orbital solutions using only HST data and a single ground-based observation set, either OGS on October 19, CFHT on October 22, or VLT on October 25. In all three tests, non-gravitational motion was detected at a significance of at least 12σ.

The vast majority of astrometric positions for 'Oumuamua were measured relative to the Gaia DR1 catalog, which does not include the proper motions of stars. Since Gaia DR1 uses 2015 as the reference epoch, offsets due to proper motions[34] could amount to as much as $\sim 0.04''$. We tested the impact of this effect by limiting our analysis to a single astrometric position for each of the four HST visits and a single OGS position on October 19, and added $\sim 0.04''\sqrt{5 \times 2}$ in quadrature to the astrometric uncertainties to account for the cumulative effect of missing proper motions. We still found a 5.3σ detection of A_1. Incidentally, we note that a remeasurement of all the data versus the newly released Gaia DR2 catalog (which does include proper motions) would not significantly alter the conclusions of this work, because other sources of biases, such as plate distortions, or timing issues, could still be present and affect the astrometry at the level taken into account by this test.

To rule out the possibility that the detection of non-gravitational motion could be due to issues with HST data (such as in the case of comet C/2013 A1 where the HST astrometry was found to have larger errors than expected[36]), we performed a fit using only ground-based observations and still detected non-gravitational motion at 7.3σ significance.

To make sure that the high significance of the detected non-gravitational signal is not caused by overly optimistic assumptions regarding the astrometric uncertainties, we used an uncertainty floor of $1''$ and still obtained a 7.0σ signal for A_1.

The results of our tests show that the observed non-gravitational signature is not an artifact of biases in the data or the specifics of the analysis performed, but is indeed present in the motion of 'Oumuamua.

Non-gravitational models. In addition to $A_1 g(r)$, with $g(r) \propto r^{-2}$, we considered several alternative models for the observed non-gravitational acceleration of 'Oumuamua. The

χ^2 and reduced χ^2 values of the corresponding fits to all astrometric data are shown in Table 1 for comparison with the gravity-only reference model. A brief summary of each model (numbered as in Table 1) is provided below:

1.   We searched for evidence of an impulsive Δv event and found two χ^2 minima, one on 2017 November 5 and another on 2017 December 7, both requiring a Δv of 5 m s $^{-1}$ or more. However, the corresponding orbital solutions provide a poorer fit to the data than continuous acceleration models. Moreover, as discussed before, evidence of non-gravitational acceleration is found in the arcs prior to 2017 December 7 and after 2017 November 5. Therefore, an impulsive Δv event alone cannot model the trajectory of 'Oumuamua.

2.   We tested different power laws for for the radial dependency of the acceleration; $g(r) \propto r^{-k}$, $k = 0,1,2,3$. A constant $g(r)$ ($k = 0$) provides a poorer fit to the data. Within our fit timespan, which extends from $r = 1.1$ au to $r = 2.9$ au, the acceleration decreases with increasing heliocentric distances at a rate that cannot be much steeper than r^{-2}, but can be gentler, e.g., r^{-1}, with both trends having comparable likelihood. A trend going with r^{-3}, on the other hand, is again strongly disfavored by the data.

3.   Adding transverse, $A_2 g(r)$, and normal (out-of-plane), $A_3 g(r)$, acceleration components to a radial-acceleration-only model (the result is referred to as the RTN model) yields only a modest improvement of the fit, regardless of the dependence with heliocentric distance we select, showing that the non-gravitational acceleration of 'Oumuamua is mostly radial. The best-fit values for A_2 and A_3 are consistent with zero (significance $< 1\sigma$) and are an order of magnitude smaller than that for A_1.

4.   Alternatively, the acceleration vector can be decomposed into   Along-track, Cross-track, and Normal (ACN) components   with respect to the   trajectory   . The goodness of the resulting fit is comparable to that obtained by for the RTN. However, in the ACN frame all three directions are needed to describe the data, while a single parameter is sufficient in the RTN frame. In particular, the fit is unacceptably poor for an exclusively along-track acceleration $A_A g(r)$ with $g(r) \propto r^{-2}$.

5.   An unacceptably poor fit is obtained if the acceleration is assumed to act exclusively in the direction of the object's velocity vector   (i.e., the along-track component of the ACN frame) , with any $g(r) \propto r^{-k}$, $k = 0,1,2,3$.

6.   We also tested the possibility of a constant acceleration vector, fixed in inertial space.   Despite the larger number of estimated parameters, the resulting fit is no better than that obtained with a purely radial acceleration. Moreover, the complex rotation state of 'Oumuamua[2,3,4] is at odds with such an inertially fixed acceleration.

7.   Finally, we tested non-gravitational models involving cometary activity. A CO-driven[15] $g(r)$ behaves similarly to r^{-2} for $r < 5$ au and provides a better fit than a H $_2$O-driven[8] $g(r)$, which falls off like $r^{-2.15}$ for $r < 2.8$ au and then abruptly decays like

r^{-26}. This latter model provides a significantly improved fit if we include a time offset $\Delta T = 56$ d with respect to perihelion for the acceleration peak[37], thus moving the fast decay of $g(r)$ outside of the data arc.

We point out that the difference between χ^2 values for models within a given family (the exponent k for each of models 2, 3, 4, and 5 of Table 1) is useful to statistically evaluate how significantly some exponents are disfavored with respect to the best-fitting one of the same family.

Limits on cometary activity. We estimated that no more than $\sim$1 kg of 1 µm-sized dust grains could have been present in the direct vicinity of 'Oumuamua ($< 2.5''$ or < 750 km from the nucleus) on October 25-26[1], based on the dust limiting magnitude for dust $g > 29.8$ mag arcsec^{-2}. Here we perform the same analysis on deep stacks of the 2017 November 21, 22, and December 1 HST data in search of evidence of dust. To this end, we subtracted a copy of each image from itself after rotation by 180°. Since any dust is pushed from the nucleus by solar radiation pressure, its distribution is expected to be highly asymmetric. The self-subtraction removes the light from the nucleus and from the symmetric component, and makes the asymmetric component more prominent. The subtracted frames were further enhanced by wavelet filtering (which boosts the signal with spatial frequencies corresponding to 2 to 8 pixels) and adaptive smoothing (which smooths the signal over a region whose size is dynamically adapted such that the SNR reaches a threshold, set here to 2). Careful examination of the resulting images, shown in Fig. 1, does not reveal any sign of dust to a similar limit. The asymmetry test is particularly sensitive for the October 25-26 stack: because the Earth was only 15 above the object's orbital plane, any dust released from the nucleus since its passage through perihelion is expected to be confined to a narrowly fanning region with position angles of approximately 90 to 135. Our findings thus indicate that the original upper limit of $\sim$1 kg of 1 µm dust within 750 km on October 25 is conservative (corresponding to $g > 29.8$ mag arcsec^{-2} at the 5σ level).

In order to test this limit, a dust feature was introduced in the images, which were then re-processed using the same enhancement techniques. The feature was produced using a cometary image approximately matching the expected morphology of ejected dust for October 25 (when the geometry was the best to concentrate the dust in a narrow region), scaled to match the photometric contribution in the central 2.5''. This is illustrated in Fig. 1, indicating that the dust would indeed likely be detected.

From the orbital fits we know that the non-gravitational acceleration on 'Oumuamua on October 25 at $r = 1.4$ au was $A_1 r^{-2} = 2.7 \times 10^{-6}$ m s^{-2}. The mass m of 'Oumuamua can be estimated from the photometry[1], assuming an albedo of 0.04 (or 0.2), and a bulk density of < 500 kg m^{-3} (or 2000 kg m^{-3}) for a cometary[38] (or asteroidal[39,20] object). If the non-gravitational force is due to cometary activity, Newton's law can be used to relate the observed acceleration to the gas production rate[40], Q, via $ma = Q\zeta v_i$, where v_i is the gas ejection velocity and ζ a poorly constrained, dimensionless efficiency factor that accounts for

(among other effects) the geometry of the emission. At the heliocentric distance of 'Oumuamua on October 25 of 1.4 au, ζv_i would fall between 150 m s^{-1} to 450 m s^{-1}; in the following, we adopt 300 m s^{-1}. The resulting gas production rates, at a heliocentric distance of 1.4 au, range from 0.7 kg s^{-1} to 140 kg s^{-1} depending of the size, shape, and mass of the object, with a mass loss of $Q = 10$ kg s^{-1} being our best estimate. This value was used to constrain the thermal model discussed in the following.

Thermal model.   We carried out thermal model calculations to estimate the interior temperatures that 'Oumuamua reached during its passage. These thermal calculations begin four years before perihelion and end two years after perihelion. The one-dimensional[5] model resolves the diurnal cycle with at least 288 time steps within each 7.34-hour simple rotation. We assumed an albedo of 0.05 and an obliquity of 45 , and used two parameter combinations: one with a porosity of 40% and a thermal inertia of 400 J m^{-2} K^{-1} s$^{-1/2}$ (at 200 K) and the other with a porosity of 90% and a thermal inertia of 40 J m^{-2} K^{-1} s$^{-1/2}$. Calculations were carried out for the object's equator (where the surface normal is perpendicular to the rotation axis), and at a latitude of 45 , starting from an initial temperature of 4 K. The depths to maximum temperature along the orbit depend on the assumed physical properties, but for the parameters specified above, which capture a wide range of values, 160 K (the approximate activation threshold for H_2O driven cometary activity) are reached roughly within the top 1 m of the surface, consistent with previous results[5]. As 'Oumuamua is only tens of meter wide, 30 K (the approximate threshold for CO activity) was exceeded within most of the body. The case of CO_2 lies in between (80 K). The model temperatures suggest that if CO ice was present, significant outgassing occurred, and even CO_2 ice would have experienced significant sublimation.

Outgassing models. In order to verify whether cometary activity can produce the observed non-gravitational acceleration, we modeled[16] the object as a comet. Note that, because of the large range of plausible masses for the nucleus, our results should be considered order-of-magnitude estimates. We assumed the following initial physical characteristics for a spherical nucleus[1]: a radius of 102 m, an albedo p of 0.04, a density ρ of 500 kg m^{-3}, an ice-to-dust ratio of unity (in mass), 60% porosity, and a bulk thermal conductivity of 0.7 W m^{-1} K^{-1}, all typical values for comets[16]. The model considers sub-surface H_2O and CO ices (with CO/$H_2O = 0.05$ by mass) and, following this model nucleus along 'Oumuamua's trajectory , evaluates the sublimation over a 400-day period centered on perihelion. The water production rate was found to peak close to perihelion and then decline following a $\sim r^{-2}$ profile until 100 days after perihelion (at 2.6 au in mid-December 2017), when it starts to decrease sharply. At that point, the CO production rate, which does not change much along the trajectory, becomes dominant, and hence the total production rate continues to follow the $\sim r^{-2}$ trend. The gas velocity was estimated at $v_i = 500$ m s^{-1}, within the range of ζv_i values discussed above.

Additional physical parameters characterizing the model nucleus (e.g., thermal conductivity, ice-to-dust ratio, bulk density) were adjusted in an attempt to match $Q_{H_2O} = 10$ kg s^{-1} at 1.4 au, our estimate of the gas production rate required to generate the observed

non-gravitational acceleration. The closest match to the observations resulted from the following model parameters: ρ = 450 kg m^{-3}, ice/dust (by mass) = 3, CO/H$_2$O = 0.25, 60% porosity. for the initial composition and low temperature. The resulting model parameters are mostly within acceptable limits and physically meaningful; for instance, the required thermal conductivity matches that of silicates, rather than that of a mix of silicate and organics. The dust production was estimated using a low drag coefficient, acknowledging that the gas, and therefore the dust, would come from the sub-surface. For our initial model, however, $Q_{\mathrm{dust}} =$ 0.2 kg s^{-1}, and the maximal gas production at 1.4 au is $Q_{\mathrm{H}_2O} = 2.5$ kg s^{-1}, which provides insufficient acceleration. With a much higher CO/H$_2$O ice ratio the production rate increases to within about a factor of 2-3 that needed to match the acceleration detected, with a dust production rate of 0.4 kg s^{-1}. A further increase in mass loss by approximately 30% would result if the surface area had an ellipsoidal shape instead of a spherical shape, with the same median photometric cross-section. The dust production rates inferred from the thermal models require the grains to be relatively large (~ 100 to mm), in order to match the optical non-detection limits for dust. Large grains are typical of outgassing from sub-surface layers as seen in laboratory experiments[41], and models of the physical interaction of Oort cloud comets and the interstellar medium show that small grains are efficiently removed by drag effects[42]. No model using an asteroid-like density[20] could be made to produce sufficient acceleration. Further, a high bulk density imposes a limit on ice content even for near zero porosity. Even assuming a very high CO/H$_2$O ratio, the maximum outgassing is over an order of magnitude too low. Finally, acceleration from outgassing would reach the required value if the assumed density of `Oumuamua is lowered to around 200 kg m^{-3}. Although other values could be obtained by adjusting the dust size distribution and the nucleus pore size, further exercises would be of little benefit, as long as we do not have additional constraints.

In conclusion, we find that sublimation can account for the measured non-gravitational forces, when modeling `Oumuamua as a small comet, but only if it has some unusual properties.

**Consequences of the analysis for the study of `Oumuamua's origin.**  The many uncertainties and assumptions in the non-gravitational models presented in this analysis have significant implications on our capabilities to fully determine the past history of `Oumuamua. These limitations are intrinsically due to the absence of observational information on the behavior of the non-gravitational acceleration outside the observed arc, and cannot be mitigated by a better analysis of the existing data (e.g., by remeasuring them in relation to the newly released Gaia DR2 catalog), since they do not provide any information on the earlier epochs. In particular, the absence of information on the behavior of the non-gravitational acceleration before the time of discovery implies that it is much more difficult (and subject to much larger uncertainties) to extrapolate the motion of `Oumuamua to its original incoming direction.

Solar radiation pressure. A simple radial dependency of the non-gravitational acceleration, decaying as $A_1 r^{-2}$ with the heliocentric distance, is allowed by the dataset for

$A_1 = (5.01 \pm 0.16) \times 10^{-6}$ m s $^{-2}$. If interpreted as solar radiation pressure on the projected area of the object exposed to sunlight, this A_1 value would correspond to an Area to Mass Ratio (AMR) between ~ 0.5 m ^{2} kg $^{-1}$ and 1 m ^{2} kg $^{-1}$. Given the range of possible sizes and shapes of 'Oumuamua[1], and assuming a uniform density and an ellipsoidal shape for the body, this estimate of the AMR would correspond to a bulk density of the object between ~ 0.1 kg m $^{-3}$ and ~ 1 kg m $^{-3}$, three to four orders of magnitude less than that of water. Alternatively, to be composed of materials with densities comparable to normal asteroidal or cometary matter (~ 1000 kg m $^{-3}$), 'Oumuamua would need to be a layer, or a shell, at most a few millimeters thick, which is not physically plausible.

Unless 'Oumuamua has physical properties that differ dramatically from those of typical Solar System bodies within the same size range, the interpretation of the non-gravitational acceleration being due to solar radiation pressure is therefore unlikely.

Binary object or fragmentation event. The existence of one or more fragments could theoretically explain the detected astrometric offsets by displacing the center of mass of the overall system from the main component that was measured astrometrically. However, the existence of a bound secondary body of significant mass can be easily discounted both directly and indirectly.

The offsets from a gravity-only solution (see Fig. 2) observed at the time of our deepest images are at the arcsecond level, requiring a possible bound, secondary body to have a separation from the main mass that is of comparable or greater size. No co-moving object was detected in the vicinity of the main body though, although most of the images we obtained with large-aperture telescopes have sub-arcsecond resolution and reach a depth a few magnitudes fainter than 'Oumuamua. Specifically, the limiting magnitudes estimated from the SNR of 'Oumuamua on deep stacks of data from the VLT (October 25) and HST (November 21 and 22) are $r'_{lim} = 27.0$ and $V_{lim} = 29.2$), respectively. Conversion to an upper limit for the radius of an unseen object yields 7.8 m (3.5 m) and 4.5 m (2.0 m) respectively, for an albedo of 0.04 (0.2) (typical values for a cometary nucleus and an asteroid), i.e., ~ 100 times smaller than the main body using the same assumptions. In addition, given 'Oumuamua's small mass, the radius of its sphere of influence $r \sim a(m/M)^{2/5}$ (where a is the distance between the object and the Sun, m and M the masses of the object and of the Sun) is of the order of ~ 1 km, corresponding to angular separations of milliarcseconds. Any object within such a distance would be fully embedded in the main body's PSF and therefore would not contribute any detectable offset to the astrometric photocenter.

The possibility of an unbound fragment being ejected by 'Oumuamua during the observed arc can also be excluded, not just because no such fragment was seen in the deep images we obtained, but also because its dynamical effect would correspond to an impulse-like event in the trajectory, which we have already shown to be incompatible with the data.

Code availability. The JPL asteroid and comet orbit determination code used in the in-depth analysis of the possible dynamical scenarios is proprietary. However, some key results of this analysis, including the detection of a significant non-gravitational acceleration at the $\sim 30\sigma$ level, can easily be reproduced by using freely available software, such as Find_Orb by Bill Gray (https://www.projectpluto.com/find_orb.htm). The code of the comet sublimation model is a direct implementation of a published model[16]. Source code and further documentation for the type of one-dimensional thermal model used is available on GitHub[45].

Data availability. The astrometric positions and uncertainties on which this analysis is based are available in the Extended Data section of the paper, and will also be submitted to the Minor Planet Center for public distribution.

References

[31] Krist, J.E., Hook, R.N., Stoehr, F.   20 years of Hubble Space Telescope optical modeling using Tiny Tim. In: Kahan, Mark A. (Ed.), Optical Modeling and Performance Predictions V. *Proceedings of the SPIE* **8127**, 16pp. (2011).

[32] Hastings, W.K.   Monte Carlo sampling methods using Markov chains and their applications. *Biometrika* **57**, 97-109 (1970).

[33] Lindegren, L., and 82 colleagues.   Gaia Data Release 1. Astrometry: one billion positions, two million proper motions and parallaxes. *A&A* **595** A4 (2016).

[34] Farnocchia, D., Chesley, S. R., Chamberlin, A. B., Tholen, D. J.   Star catalog position and proper motion corrections in asteroid astrometry. *Icarus* **245** 94-111 (2015).

[35] Monet, D. G., and 28 colleagues. The USNO-B Catalog. *AJ* **125**, 984-993 (2003).

[36] Farnocchia, D., Chesley, S. R., Micheli, et al. High precision comet trajectory estimates: The Mars flyby of C/2013 A1 (Siding Spring). *Icarus* **266** 279-287 (2016).

[37] Yeomans, D. K., Chodas, P. W.   An asymmetric outgassing model for cometary nongravitational accelerations. *AJ* **98**, 1083-1093 (1989).

[38] A'Hearn, M.F.   Comets as building blocks. Ann. Rev. Astron. Astrophys. **49**, 281-299 (2011).

[39] Carry, B.   Density of asteroids. *Planetary and Space Science* **73**, 98-118 (2012).

[40] Crovisier, J., Schloerb, F.P.   The study of comets at radio wavelengths, in *Comets in the Post-Halley era*, Ed. R.L. Newburn, M. Neugebauer and J. Rahe, Kluwer, The Netherlands, p. 166 (1991).

[41] Laufer, D., Pat-El, I. and Bar-Nun, A.   Experimental simulation of the formation of non-circular active depressions on comet Wild-2 and of ice grain ejection from cometary surfaces. *Icarus* **178**, 248-252 (2005).

[42] Stern, S.A.   ISM-induced erosion and gas-dynamical drag in the Oort Cloud. *Icarus* **84**, Issue 2, 447-466 (1990).

[43] Vereš, P., Farnocchia, D., Chesley, S. R., Chamberlin, A. B.   Statistical analysis of astrometric errors for the most productive asteroid surveys. *Icarus* **296**, 139-149 (2017).

[44] Prialnik, D.   Crystallization, sublimation, and gas release in the interior of a porous comet nucleus. *ApJ* **388**, 196-202 (1992).

[45] Schörghofer, N.   Planetary-Code-Collection: Thermal and Ice Evolution Models for Planetary Surfaces v1.1.4., GitHub, doi:10.5281/zenodo.594268, https://github.com/nschorgh/Planetary-Code-Collection/ (2017).

Extended Data
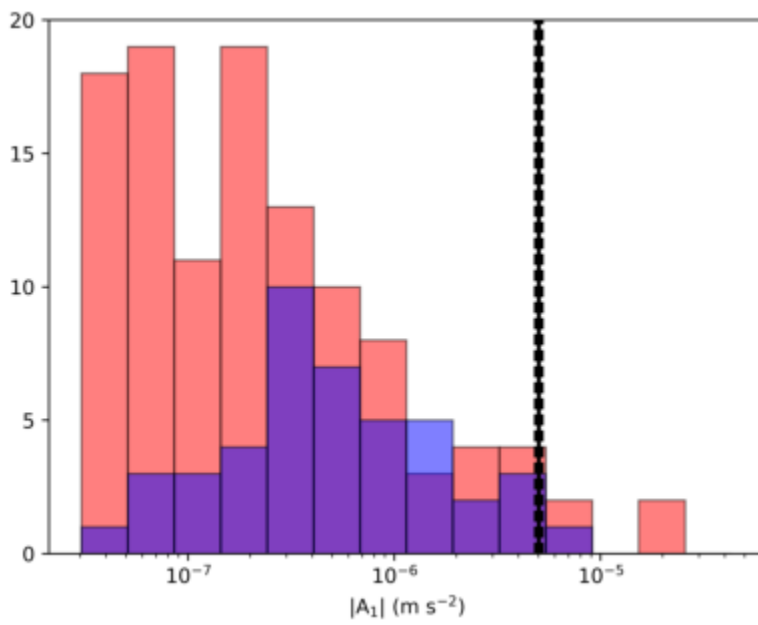
Figure 3. Non-gravitational accelerations of Solar System comets and 'Oumuamua. Measured non-gravitational radial accelerations A_1 for short-period (red) and long-period (blue) comets from the JPL Small Body Database. The solid vertical black line indicates the A_1 value for 'Oumuamua, which falls within the range observed for Solar System comets, while the dashed vertical black lines mark the corresponding 1σ uncertainty.

Table 2: Ground-based astrometric positions obtained by our team, with associated 1σ errors, as used in the analysis presented in this work. For observations with code F51 and J04 we list the manual re-measurements and associated astrometric errors that were used in this work, rather than the values available from the Minor Planet Center.

Date (UTC)	R.A.	Dec.	$\sigma_{R.A.}$ ('')	$\sigma_{Dec.}$ ('')	Obs. code
2017-10-18.472979	01 59 57.458	+02 06 04.03	1.00	1.00	F51
2017-10-18.499898	01 59 08.904	+02 07 20.19	1.50	1.50	F51
2017-10-19.397150	01 34 55.360	+02 45 03.10	0.50	0.50	F51
2017-10-19.408370	01 34 38.744	+02 45 28.26	0.50	0.50	F51
2017-10-19.419685	01 34 21.990	+02 45 53.40	0.50	0.50	F51
2017-10-19.431056	01 34 05.185	+02 46 18.67	1.00	1.00	F51
2017-10-19.940934	01 22 22.288	+03 03 53.76	0.20	0.20	J04
2017-10-19.943901	01 22 18.372	+03 03 59.57	0.20	0.20	J04
2017-10-22.371415	00 40 57.811	+04 02 50.75	0.05	0.05	568
2017-10-22.372590	00 40 56.872	+04 02 52.02	0.05	0.05	568
2017-10-22.373983	00 40 55.759	+04 02 53.50	0.05	0.05	568
2017-10-23.384311	00 28 51.402	+04 19 02.23	0.15	0.15	568
2017-10-23.385548	00 28 50.594	+04 19 03.42	0.15	0.15	568
2017-10-23.386852	00 28 49.727	+04 19 04.56	0.15	0.15	568
2017-10-25.044458	00 13 18.795	+04 39 35.18	0.05	0.05	309
2017-10-25.050182	00 13 15.977	+04 39 38.75	0.05	0.05	309
2017-10-25.061553	00 13 10.390	+04 39 45.91	0.05	0.05	309
2017-10-25.112088	00 12 45.650	+04 40 17.24	0.05	0.05	309
2017-10-25.117597	00 12 42.965	+04 40 20.67	0.05	0.05	309
2017-10-26.133749	00 05 15.166	+04 49 55.61	0.05	0.05	309
2017-10-26.138575	00 05 13.174	+04 49 58.02	0.05	0.05	309
2017-10-26.143286	00 05 11.228	+04 50 00.46	0.05	0.05	309
2017-10-26.185052	00 04 54.096	+04 50 21.88	0.05	0.05	309
2017-10-27.269327	23 58 14.606	+04 58 44.33	0.06	0.06	568
2017-10-27.282873	23 58 09.917	+04 58 50.37	0.06	0.06	568
2017-10-27.304553	23 58 02.426	+04 58 59.96	0.05	0.05	568
2017-10-27.330214	23 57 53.596	+04 59 11.17	0.05	0.05	568
2017-10-27.381822	23 57 35.927	+04 59 33.54	0.10	0.10	568
2017-11-15.306018	23 18 51.737	+06 14 13.53	0.06	0.06	568
2017-11-15.309275	23 18 51.632	+06 14 14.12	0.06	0.06	568
2017-11-15.312534	23 18 51.529	+06 14 14.68	0.06	0.06	568
2017-11-15.315806	23 18 51.415	+06 14 15.28	0.06	0.06	568
2017-11-16.207482	23 18 27.238	+06 16 59.14	0.10	0.10	568
2017-11-16.210740	23 18 27.140	+06 16 59.77	0.10	0.10	568
2017-11-16.213997	23 18 27.043	+06 17 00.37	0.10	0.10	568
2017-11-16.217253	23 18 26.952	+06 17 01.00	0.10	0.10	568
2017-11-21.026940	23 17 05.962	+06 32 01.77	0.10	0.10	304
2017-11-21.032458	23 17 05.891	+06 32 02.87	0.10	0.10	304
2017-11-21.038153	23 17 05.830	+06 32 04.05	0.10	0.10	304
2017-11-21.043922	23 17 05.761	+06 32 05.12	0.10	0.10	304
2017-11-21.060925	23 17 05.573	+06 32 08.23	0.10	0.10	304
2017-11-21.066145	23 17 05.522	+06 32 09.16	0.10	0.10	304
2017-11-21.081650	23 17 05.345	+06 32 12.19	0.10	0.10	304

2017-11-22.222847	23 16 57.163	+06 35 44.30	0.05	0.05	568
2017-11-22.246144	23 16 56.974	+06 35 48.66	0.05	0.05	568
2017-11-22.269437	23 16 56.787	+06 35 53.19	0.05	0.05	568
2017-11-22.292688	23 16 56.600	+06 35 57.56	0.05	0.05	568
2017-11-22.316355	23 16 56.413	+06 36 02.01	0.05	0.05	568
2017-11-23.038940	23 16 53.143	+06 38 25.82	0.15	0.15	304
2017-11-23.070610	23 16 52.968	+06 38 32.12	0.15	0.15	304
2017-11-23.274337	23 16 52.323	+06 39 06.39	0.06	0.06	568
2017-11-23.288299	23 16 52.246	+06 39 09.10	0.10	0.10	568
2017-11-23.373957	23 16 51.838	+06 39 25.53	0.12	0.12	568

Table 3. Full set of HST-based astrometric positions used in this work, together with the corresponding geocentric location of the spacecraft in equatorial J2000.0 Cartesian coordinates. Uncertainties of $0.05''$ were assumed for these observations in our orbital analysis.

Date (UTC)	R.A.	Dec.	X (km)	Y (km)	Z (km)
2017-11-21.139509	23 17 05.3955	+06 32 22.632	+1805.5	−6039.4	−2856.3
2017-11-21.145770	23 17 05.1365	+06 32 24.563	+4951.8	−3534.9	−3298.1
2017-11-21.152032	23 17 04.8175	+06 32 25.151	+6405.6	+0177.8	−2609.7
2017-11-21.158293	23 17 04.5287	+06 32 24.595	+5667.8	+3829.1	−1026.1
2017-11-21.164555	23 17 04.3526	+06 32 23.495	+2987.7	+6167.8	+0909.8
2017-11-21.205724	23 17 04.8236	+06 32 35.189	+1802.8	−6034.8	−2867.8
2017-11-21.211986	23 17 04.5646	+06 32 37.105	+4953.8	−3533.6	−3296.4
2017-11-21.218247	23 17 04.2473	+06 32 37.678	+6411.5	+0175.0	−2595.4
2017-11-21.224509	23 17 03.9617	+06 32 37.122	+5675.7	+3823.3	−1004.2
2017-11-21.230770	23 17 03.7868	+06 32 36.027	+2994.8	+6161.0	+0932.0
2017-11-22.530365	23 16 55.8275	+06 36 47.913	+1967.4	−5863.4	−3105.7
2017-11-22.536627	23 16 55.5977	+06 36 49.505	+5137.0	−3351.2	−3205.3
2017-11-22.542888	23 16 55.3148	+06 36 49.835	+6550.5	+0306.2	−2206.4
2017-11-22.549150	23 16 55.0666	+06 36 49.179	+5722.2	+3858.3	−0450.5
2017-11-22.555411	23 16 54.9267	+06 36 48.188	+2932.4	+6087.4	+1460.0
2017-12-12.064697	23 20 53.3769	+07 45 46.677	+1688.5	−6657.7	+0799.1
2017-12-12.070959	23 20 53.4114	+07 45 47.319	+4672.0	−4470.3	+2446.9
2017-12-12.077220	23 20 53.3938	+07 45 48.340	+6053.5	−0749.6	+3253.5
2017-12-12.083482	23 20 53.3821	+07 45 49.866	+5359.7	+3228.0	+2941.7
2017-12-12.089743	23 20 53.4285	+07 45 51.884	+2828.8	+6098.9	+1618.8
2018-01-02.320638	23 31 48.3208	+09 16 31.399	+1649.4	−6505.8	+1652.0
2018-01-02.326900	23 31 48.4827	+09 16 34.208	+4860.4	−4912.3	−0234.9
2018-01-02.333161	23 31 48.5961	+09 16 36.862	+6404.0	−1633.3	−2041.0
2018-01-02.339423	23 31 48.7029	+09 16 39.028	+5753.9	+2205.5	−3146.2
2018-01-02.345684	23 31 48.8403	+09 16 40.568	+3135.8	+5290.2	−3172.6
2018-01-02.453080	23 31 53.0509	+09 17 08.129	+1646.0	−6517.8	+1607.9
2018-01-02.459342	23 31 53.2127	+09 17 10.953	+4850.5	−4919.4	−0285.4
2018-01-02.465603	23 31 53.3284	+09 17 13.588	+6391.2	−1633.3	−2080.6
2018-01-02.471865	23 31 53.4343	+09 17 15.751	+5742.7	+2213.0	−3161.5
2018-01-02.478126	23 31 53.5702	+09 17 17.257	+3129.9	+5302.3	−3158.1

Table 4: Adopted uncertainties for astrometry obtained by other observers and publicly available through the Minor Planet Center. For all observations not listed in this table we conservatively[43] adopted uncertainties of $1''$. Observations marked with a star in the error columns were deemed unreliable by the respective observers and hence excluded from our analysis. Finally, the listed uncertainties for 703, H01, and G37 were obtained through direct communication with the corresponding observers.

Obs. code	Date (UTC)	$\sigma_{R.A.}$ ($''$)	$\sigma_{Dec.}$ ($''$)
703	2017 October 14, 17	2	2
246	2017 October 19	3	3
Q62	2017 October 22	3	3
G96	2017 October 25	*	*
850	2017 October 27	6	6
H01	2017 October 28, 29, 30	0.3	0.3
705	2017 October 29	3	3
G37	2017 October 30	*	*
H01	2017 November 9, 10, 12	0.3	0.3
G37	2017 November 11	0.3	0.3
H01	2017 November 17	0.5	0.5